Applied Catalysis B: Environmental 140–141 (2013) 179–188

Contents lists available at SciVerse ScienceDirect

Applied Catalysis B: Environmental

journal homepage: www.elsevier.com/locate/apcatb

A BiOCl film synthesis from Bi_2O_3 film and its UV and visible light photocatalytic activity

Kan Li [a], Yanping Tang [b], Yunlan Xu [c], Yalin Wang [a], Yuning Huo [d], Hexing Li [d], Jinping Jia [a,*]

[a] School of Environmental Science and Engineering, Shanghai Jiao Tong University, Shanghai, 200240, PR China
[b] School of Chemistry and Chemical Engineering, Shanghai Jiao Tong University, Shanghai, 200240, PR China
[c] School of Chemistry and Chemical Engineering, Chongqing University of Technology, Chongqing, 400050, PR China
[d] Department of Chemistry, Shanghai Normal University, Shanghai, 200234, PR China

ARTICLE INFO

Article history:
Received 21 January 2013
Received in revised form 22 March 2013
Accepted 1 April 2013
Available online 7 April 2013

Keywords:
BiOCl film
Bi_2O_3 film
Photocatalysis
Rhodamine B
Dye sensitization

ABSTRACT

A facile method was proposed to prepare BiOCl film on a Ti substrate using Bi_2O_3 film reacting with Cl^- in acidic condition. The as-prepared BiOCl film was characterized by X-ray diffraction (XRD), field emission scanning electron microscope (FESEM), high-resolution transmission electron microscopy (HRTEM) and UV–vis diffuse reflectance spectra (UV–vis DRS). The BiOCl film owned a hierarchical nanostructure and a nucleation–dissolution–recrystallization growth mechanism was observed according to the FESEM at different reaction time. The photocatalytic activity of the BiOCl film was investigated by degradation of 50 mL 5 mg L^{-1} Rhodamine B (RB) solution under UV and visible light, strong adsorption capacity (more than 10% RB adsorbed on the surface before light on) and excellent photocatalytic performance were observed. 100% and more than 90% color removal efficiencies were achieved under UV and visible light in 120 min and 180 min, better than that obtained by TiO_2 film, especially under visible light. Meanwhile more than 90% and 70% TOC could also be removed under UV and visible light in the same condition. The analysis of RB photocatalytic degradation mechanisms suggested that the prepared BiOCl film exhibited high activity for direct semiconductor photoexcitation RB degradation under UV light, while it also possessed superior activity for indirect RB photosensitization degradation under visible light. The prepared BiOCl film also exhibited excellent photocatalytic activity for other dye solutions and possessed the potential application in wastewater treatment.

1. Introduction

Recently, Bi-based compounds such as Bi_2O_3 [1], BiOX (X = Cl, Br, I) [2], Bi_2WO_6 [3] and $BiVO_4$ [4], have received great interest in photocatalytic degradation organic pollutants. Among which, bismuth oxychloride (BiOCl), as one of the important main group V–VI–VII multicomponent metal oxyhalide, has drawn particular attention in applications such as cosmetics [5], ferroelectreic materials [6], catalysts [7] and photoelectrochemical devices [8] due to its unique and excellent optical, catalytic, electrical, magnetic and luminescent properties and the extremely low toxicity. Meanwhile many researchers have revealed that nanostructured BiOCl exhibits great photocatalytic degradation performance under UV light irradiation, even better than TiO_2 [9,10]. Furthermore, some dye molecules such as Rhodamine B and Methylene Green can easily adsorb on the surface of BiOCl and further be degraded under visible light irradiation due to the dye sensitization [11,12].

Owing to its unique properties and promising applications, there is considerable interest in improved BiOCl systems. Various nanostructures including nanobelts, nanowires, nanosheets, nanofibers and nanoflowers have been fabricated via various synthetic routes, such as template-assisted synthesis [13], hydro/solvothermal method [14], sonochemistry [15], electro spinning [16], ionothermal synthesis [17] and so on. Though nanostructured BiOCl owns high photocatalytic activity, similar to TiO_2, it is difficult to separate and recycle when BiOCl was performed in liquid phase with suspended photocatalyst powder, which makes it hard to be applied to continuous flow system. Moreover, BiOCl has a bigger molecular weight than TiO_2 and is much easier to sediment and aggregate in solution, which is also a drawback for the application. Compared with BiOCl powders and particles, BiOCl film exhibits advantages such like easy recovery and recycling, no aggregation and easy surface modification. In addition, BiOCl film also has the potential applications in the cosmetic, optoelectronic and photovoltaic fields. However there have been very few reports on the fabrication of BiOCl film with nanostructure. Peng et al. [18] developed a vapor-phase synthesis route for the direct growth of high quality BiOCl nanostructure films on various substrates by thermal evaporation of a $AuCl_3$/Bi mixture or $BiCl_3$ at low-temperature (250 °C).

* Corresponding author. Tel.: +86 21 54742817; fax: +86 21 54742817.
E-mail address: jpjia@sjtu.edu.cn (J. Jia).

0926-3373/$ – see front matter © 2013 Elsevier B.V. All rights reserved.
http://dx.doi.org/10.1016/j.apcatb.2013.04.005

They found that the morphologies of the BiOCl films including nanowires, nanobelts, nanoflowers, nanoflakes and platelets could be controlled by choosing the deposition temperature, evaporation source and catalysts. Cao et al. [19] fabricated a BiOCl film with flower-like hierarchical structures by dipping Bi film in a mixed solution of H_2O_2 and HCl. The new film exhibited excellent photoluminescence property, indicating potential applications in optoelectronic devices. However the photocatalytic performances of the BiOCl films that synthesized were not investigated by both of them. Wu et al. [20] synthesized BiOCl flake and nanowire arrays on anodic aluminum oxide (AAO) templates via sol–gel combined with the vacuum air-extraction method using BiOCl powder as raw material. High photocatalytic activity was confirmed for the BiOCl film that synthesized on decomposition of Rhodamine B under UV irradiation. Zhang et al. [21] prepared a BiOCl film with highly exposed (1 1 0) surface through electrochemical method composed of a cathodic electrodeposition and an anodic oxidation at room temperature. The synergistic effect between BiOCl bulk and BiOCl (1 1 0) surface accelerated the efficient separation of electron–hole pairs, which caused the efficient photodegradation of Methyl Orange under UV irradiation. However in most cases, a Bi film would be synthesized first before the fabrication of BiOCl film, which caused complicated synthesize process and high cost. It is still a big challenge to develop a facile and environmental friendly route to prepare BiOCl film. Meanwhile because UV light only occupies less than 5% of solar light, the performance of BiOCl film under visible light also need to be investigated and improved.

In our former work, a Bi_2O_3 film with narrow band gap energy was prepared on a Ti substrate using a facile sol–gel and dip coating method and was used to degrade Rhodamine B (RB) solution under UV and visible light irradiation, however the visible light photocatalytic activity was still very low [22]. In this study, a facile way was proposed using the Bi_2O_3 film that former synthesized, instead of a Bi film, to react with Cl^- in acidic condition to prepare a BiOCl film. The as-prepared BiOCl film was analyzed by X-ray diffraction (XRD), field emission scanning electron microscope (FESEM), high-resolution transmission electron microscopy (HRTEM) and UV–vis diffuse reflectance spectra (UV–vis DRS). The growth mechanism of the hierarchical structure BiOCl was discussed in this study and the photocatalytic activity of the BiOCl film was investigated by decomposing Rhodamine B (RB) and other dye solutions under UV and visible light irradiation using a rotating disk photocatalytic reactor, which had been confirmed to be an efficient photocatalytic reactor [23–25]. The RB photocatalytic degradation mechanisms under UV and visible light were analyzed by degrading colorless salicylic acid (SA) instead of RB, detecting photo-generated current and adding trapping agents.

2. Experimental

2.1. Preparation of BiOCl film

All chemical reagents purchased from Shanghai Chemical Reagent Co., China, were in analytical grade without further purifications. Ti substrates (a round disk with diameter of 75 mm, thickness of 1 mm, Shanghai Hongtai Metal Production Co. Ltd., China) were burnished using abrasive paper and then ultrasonic cleaned using acetone and distilled water respectively. The BiOCl film was prepared using Bi_2O_3 film in the presence of Cl^- in acidic condition and the schematic preparation process has been shown in Fig. 1. The precursor solution for Bi_2O_3 film was prepared by the following method. 4.0 g $Bi(NO_3)_3{\cdot}5H_2O$ was dissolved in 20 mL ethanol containing 1 mol L^{-1} HNO_3. After being stirred for 30 min, a transparent solution was obtained. The result solution was dip-coated onto a Ti plate and then the Ti plate was dried at 80 °C for 30 min to form a $Bi(NO_3)_3$ film. The coated Ti plate was calcined at 350 °C for 2 h with heating rate of 5 °C min^{-1}. After cooling to room temperature with the cooling rate of 5 °C min^{-1}, the light-yellow Bi_2O_3 film was obtained. The Bi_2O_3/Ti plate was then immersed in 0.1 mol L^{-1} NaCl solution with pH 2.0 for 30 min. Bi_2O_3 would react with Cl^- in acidic condition to form BiOCl and the color of the film turned from light-yellow (Bi_2O_3) to white (BiOCl).

2.2. Characterization of BiOCl film

The BiOCl powder was sonicated down from the BiOCl/Ti plate and used for further detection of X-ray diffraction (XRD), diffuse reflectance absorption spectra (DRS) and high-resolution transmission electron microscopy (HRTEM). The crystal structure of the as-synthesized BiOCl was determined by X-ray diffraction (XRD) using a D/Max2200 diffractometer (Rigaku, Japan) at a scanning rate of 5° min^{-1} in the 2θ range from 10° to 90°. The UV–vis diffuse reflectance absorption spectra (UV–vis DRS) was recorded on a Lambda 750S UV-VIS-NIR spectrophotometer (PerkinElmer, USA) in the range of 200–800 nm. The morphology of the BiOCl film was characterized by a S-2150 field emission scanning electron microscope (FESEM, Hitachi Corp., Japan) at a high voltage of 15 kV and a JSM-2010 high-resolution transmission electron microscopy

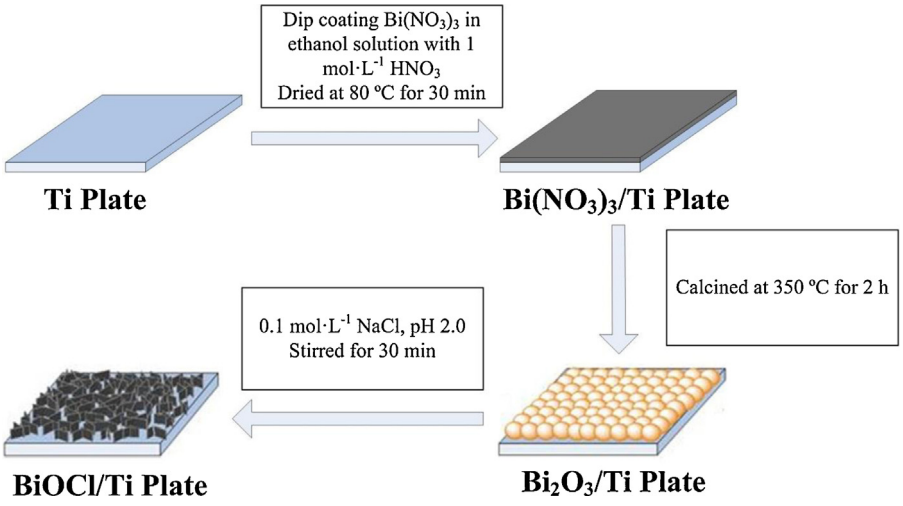

Fig. 1. The schematic of preparation process for BiOCl film.

(HRTEM, JEOL Ltd., Japan). The specimen of HRTEM measurement was prepare via spreading a droplet of ethanol suspension onto a copper grid, coated with a thin layer of amorphous carbon film, and allowed to dry in air. Linear sweep voltammograms were obtained under different experimental conditions using an Autolab 4.9 system (Metrohm, Switzerland) with the BiOCl/Ti plate as the working electrode; and Pt and saturated calomel electrodes as the auxiliary and reference electrodes.

2.3. Photocatalytic activity measurement

The photocatalytic activities of BiOCl film was evaluated through the degradation of Rhodamine B (RB) and other dye solutions using a rotating disk reactor under UV and visible light irradiation. The schematic diagram of the reactor was shown in Fig. S1. The rotating speed was set at 60 rpm which was controlled by a motor (Outai Transmission Electromechanical Co. Ltd., Shanghai, China). The reactor was placed 3 cm away from the light source. An 11 W mercury lamp (Philips, 254 nm) and a 150 W xenon lamp (Shanghai Lansheng Co. Ltd., Shanghai, China) with a 400 nm cutoff filter were used as UV and visible light source, the light intensity was maintained constantly at 13 mW cm^{-2} and 50 mW cm^{-2} respectively. 50 mL of 5 mg L^{-1} Rhodamine B (RB) solution was filled in the reactor to be treated. Before the experiment, the film was rotated in dark for 30 min to reach adsorption–desorption equilibrium. A Ti substrate and a TiO_2/Ti plate prepared by dip coating and sol–gel method (the details of the process and the properties of the film were shown in Supplementary data) were also used to compare the performance of the BiOCl film in the same condition. Meanwhile 50 mL of 10 mg L^{-1} colorless salicylic acid (SA) solution was also used instead of RB to be treated under UV and visible light irradiation respectively. In order to analyze the mechanisms of photocatalytic degradation process, the photo generated holes, •OH and $O_2^{\bullet-}$ were detected by adding trapping agents during the reaction. 1 mmol L^{-1} KI [26], 10 mmol L^{-1} tert-butyl alcohol (TBA) [27] and 0.1 mmol L^{-1} benzoquinone (BQ) [28] were used to capture photo generated holes, •OH and $O_2^{\bullet-}$ respectively. 50 mL of 5 mg L^{-1} other dye solutions, including Methylene Blue (MB), Basic Orange (BO), Methyl Orange (MO) and Reactive Brilliant Red X-3B (RBR), were also used to be treated in the same condition to evaluate the photocatalytic performance of the BiOCl film.

The concentrations of dye and SA solutions were determined by measuring solution absorbance (λ = 563 nm for RB, 665 nm for MB, 449 nm for BO, 465 nm for MO, 538 nm for RBR and 297 nm for SA respectively) using a UV–vis spectrophotometer (UV-2102PCS, UNICO, Shanghai). TOC was measured using a TOC/TN analyzer (Jena 3000, Germany) to evaluate the mineralization extent of the dye.

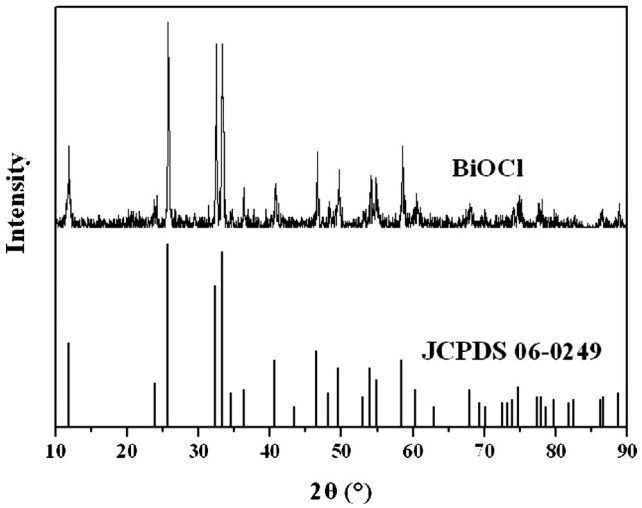

Fig. 2. XRD pattern of the BiOCl film that synthesized.

3. Results and discussion

3.1. Morphology and structure

The XRD pattern of Bi_2O_3 film that synthesized is shown in Fig. S2. The pattern matched well with the tetragonal phase of bismuth oxide (β-Bi_2O_3) with the lattice constants of $a = b = 7.740$ Å, $c = 5.632$ Å, which were consistent with the values from the standard JCPDS 27-0050. While the Bi_2O_3 film would react with Cl^- in acidic condition to form BiOCl film. Fig. 2 displays the XRD pattern of BiOCl film that prepared, all the diffraction peaks agreed well with the tetragonal structure of BiOCl (space group: *P*4/*nmm* (129), JCPDS 06-0249) with the lattice constants of $a = b = 3.891$ Å and $c = 7.369$ Å. The intense and sharp diffraction peaks suggested that the as-prepared BiOCl film had a high degree of crystallization. The Bi_2O_3 and BiOCl XRD patterns indicate that the β-Bi_2O_3 film can react with Cl^- in acidic condition to form BiOCl film.

The surface nanostructure of the BiOCl film was detected by the field emission scanning electron microscope (FESEM) and the results are shown in Fig. 3. As shown in Fig. 3, the flowerlike hierarchical structure of BiOCl was observed, which was composed of several nanopetals with 10 nm thick and 400–500 nm in plane size perpendicular to the Ti substrate. The flowerlike hierarchical micro structure not only enhances the surface area of the BiOCl film, but also utilizes the irradiation light more efficiently due to the multi-reflections on the surface [29,30].

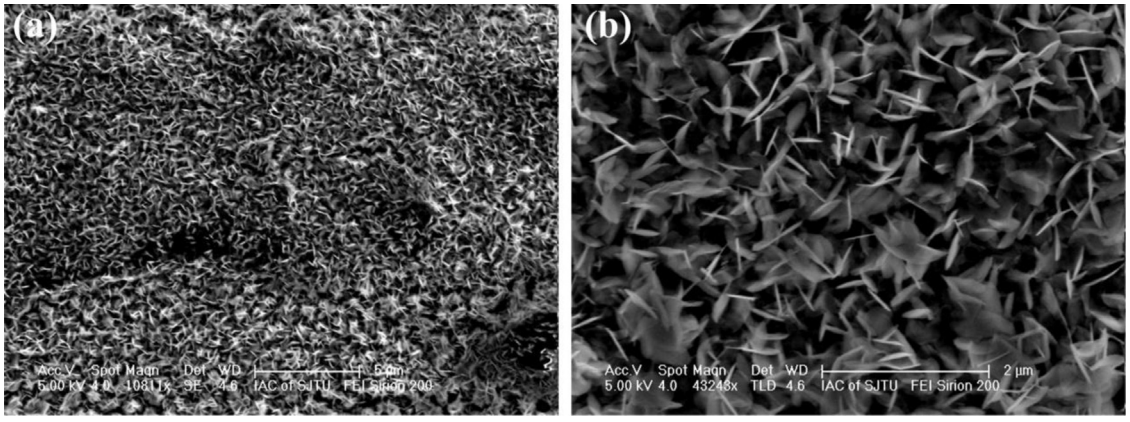

Fig. 3. FESEM images of BiOCl film with (a) low magnification and (b) high magnification.

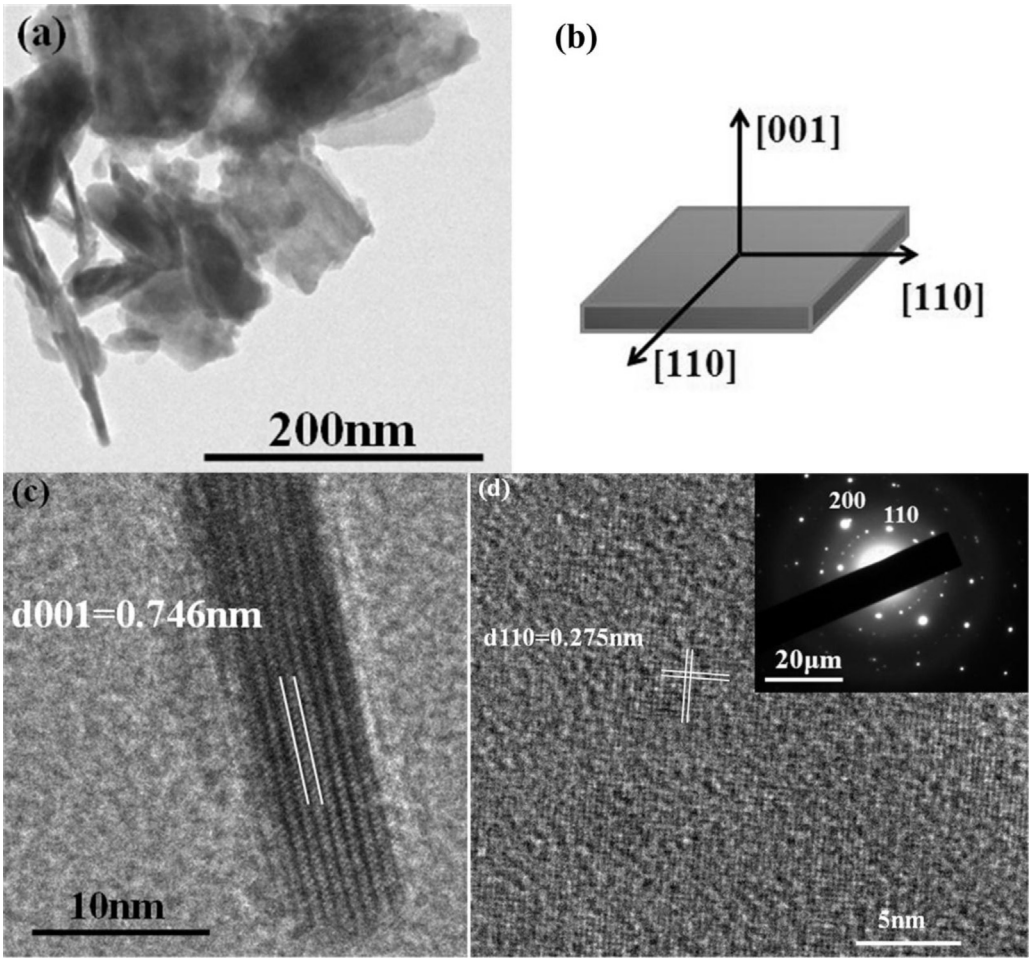

Fig. 4. (a) Low-magnification TEM image of BiOCl nanosheets. (b) Schematic illustration of the crystal orientation of the nanosheet. (c) HRTEM image of the side view of a BiOCl nanosheet, (d) HRTEM image and SAED pattern of the BiOCl nanosheet taken along the [0 0 1] zone axis.

In order to investigate the detailed crystal structure of the BiOCl flowerlike hierarchical structure, TEM and HRTEM were carried out and the results are shown in Fig. 4. After strong ultrasonication, some of the film were separated from the Ti substrate and broken into nanosheets with different sizes. As shown in Fig. 4a, most of the nanosheets were more irregular and overlapped with each other. The bottom and top surface of the BiOCl nanosheets were identified as {0 0 1} facets, while the four lateral surfaces were {1 1 0} facets (Fig. 4b). The HRTEM image of the side wall of a nanosheet is shown in Fig. 4c and visible lattice fringes of (0 0 1) planes with a lattice spacing of 0.746 nm were clearly observed. The HRTEM image of a single nanosheet (viewed from {0 0 1} axis) in Fig. 4d showed clearly two sets of lattice fringes with a lattice spacing of 0.275 nm, corresponding to that of the (1 1 0) planes. A corresponding SAED pattern (Fig. 4d inset) of a single BiOCl nanosheet was further examined and its unique pattern of diffraction spots could be indexed to the (1 1 0) and (2 0 0) plane, which confirmed its single crystal structure. The HRTEM and SAED analysis indicate that the nanosheets are single crystal and grow along the {1 1 0} orientations, with the {0 0 1} facets exposed [8,14].

The BiOCl that synthesized has a tetrahedron structure, which can derive from the fluorite (CaF_2) structure [10]. As shown in Fig. S3a, the Bi atom is coordinated with four O atoms in one base and four Cl atoms in another. The Bi and four O atoms form a tetragonal pyramid, meanwhile the Bi atom and four Cl atoms form another tetragonal pyramid in the opposite but asymmetric direction and two pyramids are interlaced. The 3D model of the BiOCl layered structure is shown in Fig. S3b, O, Bi and Cl ions stack layer upon layer in the planes perpendicular to the *c* axis to form the five-layered unit (Cl–Bi–O–Bi–Cl), which can be considered as a planar 'macromolecule' with a weak nonbonding interlayer van der Waals interaction along the *c* axis ({0 0 1} axis) and strong intralayer bonding along *a* and *b* axes ({1 1 0} axis).

3.2. Growth mechanism of BiOCl film

In order to understand the growth mechanism of the hierarchical BiOCl film in this work, FESEM images of the BiOCl film at different time stage are shown in Fig. 5. As shown in Fig. 5a, before the reaction with Cl^-, the Bi_2O_3 film was uniform, rough and consisted by the Bi_2O_3 nanosphere like particles, the size of which were 350–400 nm. After the reaction with Cl^- in acidic condition for 5 min (Fig. 5b), the Bi_2O_3 nanoshperes structure gradually disappeared and a little amount of BiOCl nanosheets were observed. However the shape of the film was still rough and indistinguishable. With the increasing of reaction time to 15 min (Fig. 5c), the film become smoother and the hierarchical structure become much clearer, however the shape of the nanosheets was incomplete with low height and the arrangement was still loose. After 30 min reaction (Fig 5d), more BiOCl nanosheets with smooth surface were formed and most of them connected with each other, grew more densely and deeply. The color of the film also changed form light-yellow (Bi_2O_3, Fig. S4a) to white (BiOCl, Fig. S4b).

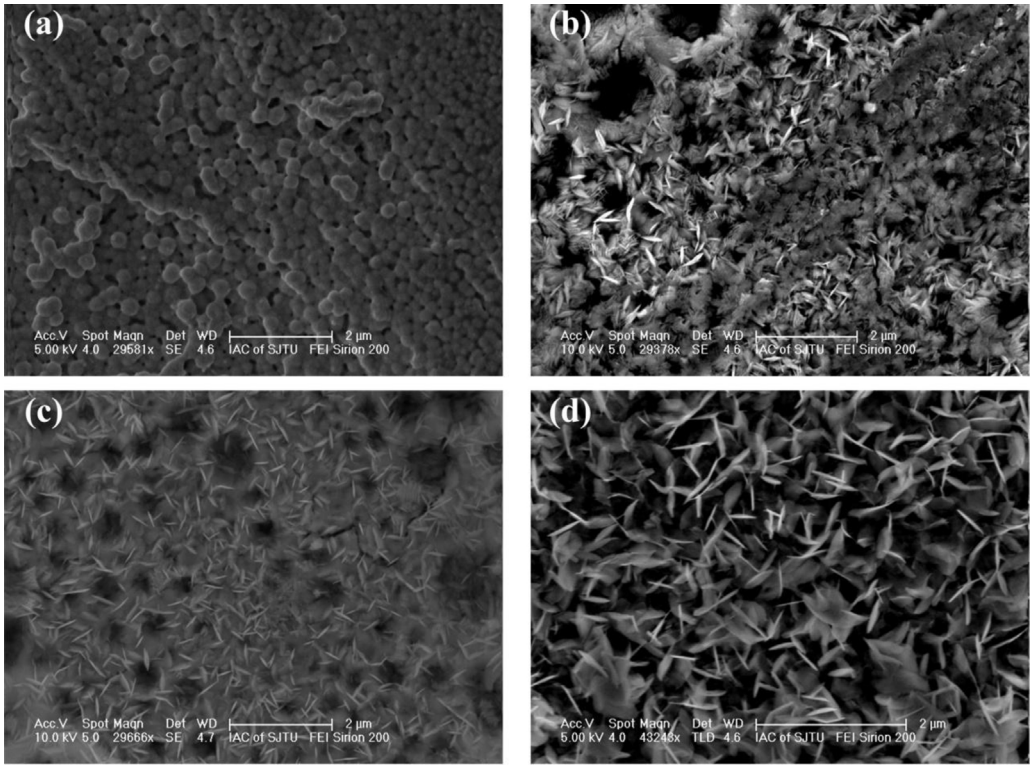

Fig. 5. FESEM images of the BiOCl film after different reaction times (a) 0 min; (b) 5 min; (c) 15 min; (d) 30 min.

In our case, because there were no hard or soft templates used to help form the hierarchical structure BiOCl film, the growth mechanism of the BiOCl film was preferred to be a nucleation–dissolution–recrystallization process, which was similar to that proposed by Cao et al. [19] using Bi film dipped in the mixed solution of H_2O_2 and HCl. The process is summarized in Fig. 6. The Bi_2O_3 on the surface of the nanospheres would react with Cl^- in acidic condition to form $BiCl_3$ (Eq. (1)) dissolved in water first. Then the dissolved $BiCl_3$ was hydrolyzed immediately in water to form BiOCl (Eq. (2)) deposited on the surface of Bi_2O_3 and acted as nucleation centers. The Bi_2O_3 in the inner part then was further dissolved and more BiOCl would be formed and grew faster on the nucleation centers along the {1 1 0} orientations rather than the {0 0 1} orientations due to the weak *c* axis bonding, leading to the generation of nanosheet structure.

$$Bi_2O_3 + 6Cl^- + 6H^+ \rightarrow 2BiCl_3 + 3H_2O \quad (1)$$

$$BiCl_3 + H_2O \rightarrow BiOCl\downarrow + 2HCl \quad (2)$$

3.3. Optical absorption property of BiOCl film

The optical absorption property of the semiconductor is one of the important factors determining its photocatalytic performance. The UV–vis diffuse reflectance spectra (DRS) of BiOCl film that prepared is shown in Fig. 7a. The onset of BiOCl was determined at 280 nm and the absorption edge occurred at about 380 nm. The magnitude of band gap of BiOCl was estimated from a curve of $(\alpha h\upsilon)^{1/2}$ versus the photon energy $h\upsilon$ with the help of Tauc relation. As shown in Fig. 7b, the band gap energy of BiOCl film that synthesized was 3.0 eV, which was lower than the theoretic value (3.46 eV). It is well known that the structure, morphology and size of the semiconductor nanostructures have an important influence on related optical properties and change the band gap energy as a result [31]. The UV–vis diffuse reflectance spectra indicates that the prepared BiOCl film can easily be excited by UV light, however will not be excited by visible light due to the wide band gap energy.

3.4. Photocatalytic activity of BiOCl film on RB removal

Many researchers have reported that BiOCl owns high activity for direct semiconductor photoexcitation pollutant degradation under UV light, while it also possesses superior activity for indirect dye photosensitization degradation under visible light due to its strong dye adsorption capacity [9–12]. In our case, the photocatalytic activity of as-prepared BiOCl film was investigated by photocatalytic degradation of 50 mL 5 mg L^{-1} Rhodamine B (RB) solution under UV and visible light, the results are shown in Fig. 8. Because TiO_2 film is widely used by many researchers as efficient photocatalyst, a TiO_2 film prepared by sol–gel and dip coating method was also used to compare and evaluate the photocatalytic performance of the BiOCl film. The XRD pattern of the TiO_2 film

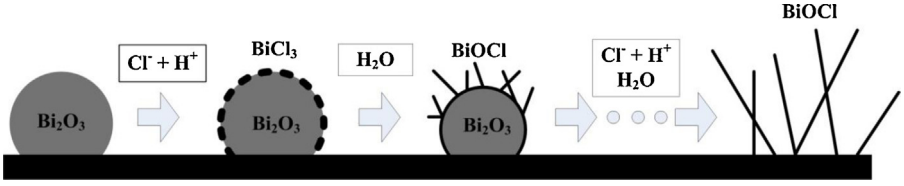

Fig. 6. Schematic illustration of the formation process of the BiOCl hierarchical structure.

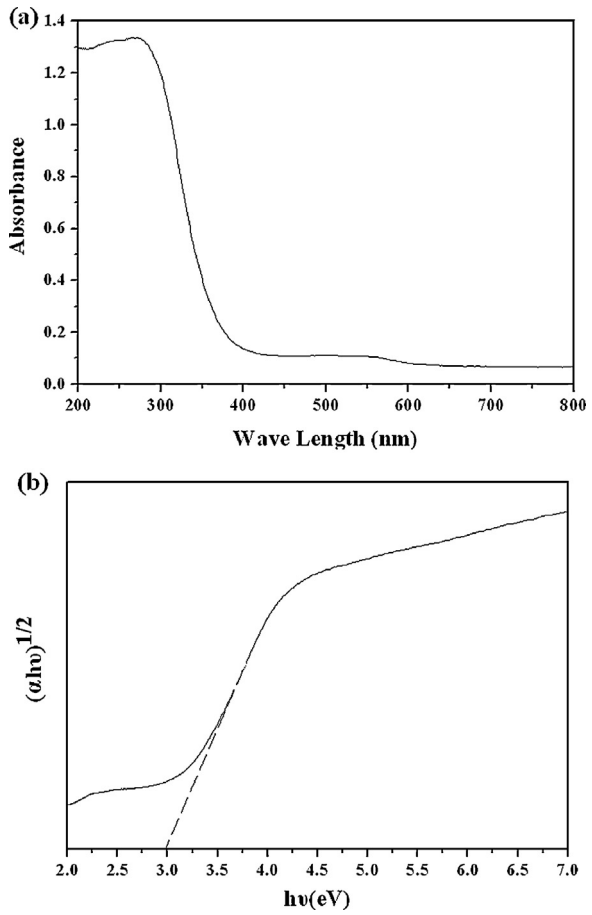

Fig. 7. (a) The UV–vis diffuse reflectance spectrum of BiOCl film and (b) the curve of $(Ah\upsilon)^{1/2}$ vs. $h\upsilon$ for BiOCl film.

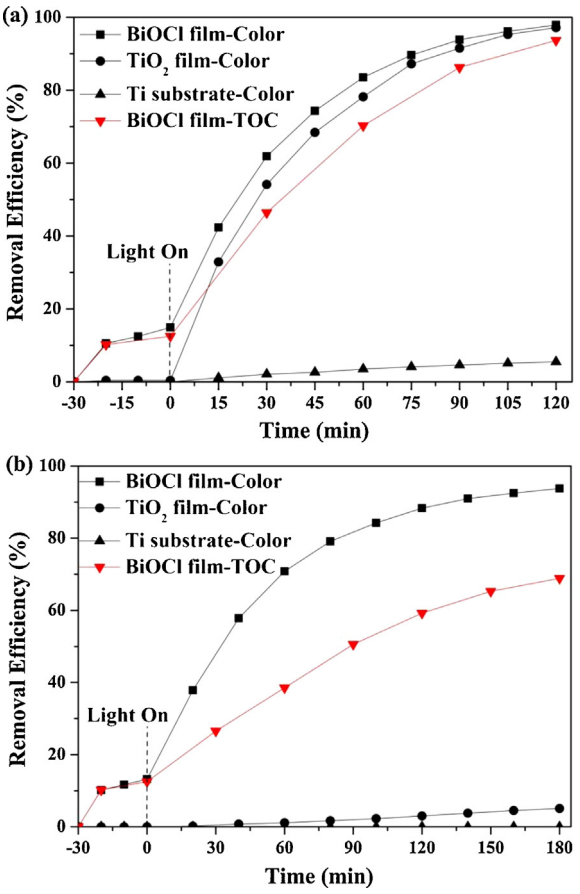

Fig. 8. The color and TOC removal of 5 mg L^{-1} RB using BiOCl film, TiO_2 film and Ti substrate under (a) UV and (b) visible light irradiation. (For interpretation of the references to color in this figure legend, the reader is referred to the web version of the article.)

provided in Fig. S5 indicates that the TiO_2 film was in anatase phase, the photocatalytic activity of which is much better than that of rutile phase.

As shown in Fig. 8, less than 5% RB could be removed in 120 min by UV or visible light photodegradation when Ti substrate was used without any catalyst immobilized on the surface. Meanwhile more than 10% RB could be adsorbed on the surface of the BiOCl film before light on, however there was no RB adsorbed on the surface of TiO_2 film. When UV light irradiates (Fig. 8a), more than 65% color was removed in 30 min for the BiOCl film and 100% color removal efficiency was achieved in 120 min. Compared with result obtained by TiO_2 film, the color removal efficiency of BiOCl film was more than 10% better at the early stage of the reaction. This result suggests that the BiOCl film that synthesized owns better UV photocatalytic performance than TiO_2 film in RB degradation. The better performance is caused by two reasons, the first is that RB can be concentrated degraded due to the strong adsorption capacity on the surface of BiOCl film; the second is that the flowerlike hierarchical micro structure not only enhances the surface area, but also utilizes the irradiation light more efficiently due to the multi-reflections on the surface [29,30]. When visible light irradiated, as shown in Fig. 8b, because TiO_2 can hardly be excited by visible light, less than 5% RB was removed in 180 min when TiO_2 film was used. However, when BiOCl film was used, more than 90% RB was removed in 180 min. Because the BiOCl film can also hardly be excited by visible light according to the result of UV–vis DSR (Fig. 7), the great visible light RB photocatalytic activity of BiOCl film may be mainly due to the dye sensitization. In order to confirm this, 50 mL 10 mg L^{-1} colorless salicylic acid (SA) solution was also be degraded using BiOCl film under UV and visible light respectively and the results are shown in Fig. 9 and Fig. S6. Because the SA has no color and can hardly be adsorbed on the surface of BiOCl film, the indirect sensitization will not take place and only less than 5% SA was removed in 120 min under visible light irradiation. However there was still 90% SA removed in 120 min under UV irradiation due to the direct semiconductor photoexitation.

Compared with aromatic ring and organic acids groups, the chromophoric group (—C═N—) of RB is much easier to be destroyed

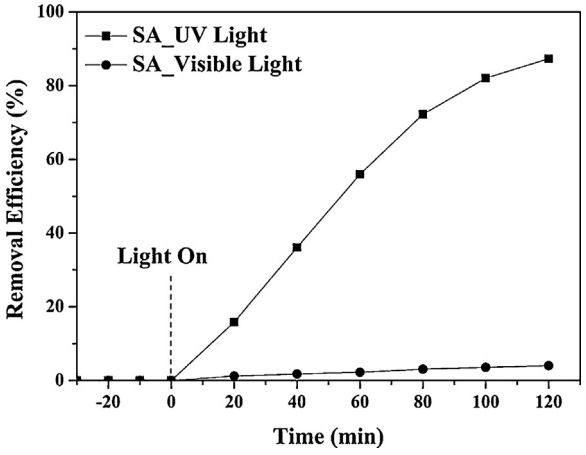

Fig. 9. The photocataytic degradation of 50 mL 10 mg L^{-1} colorless SA solution using BiOCl film under UV and visible light irradiation.

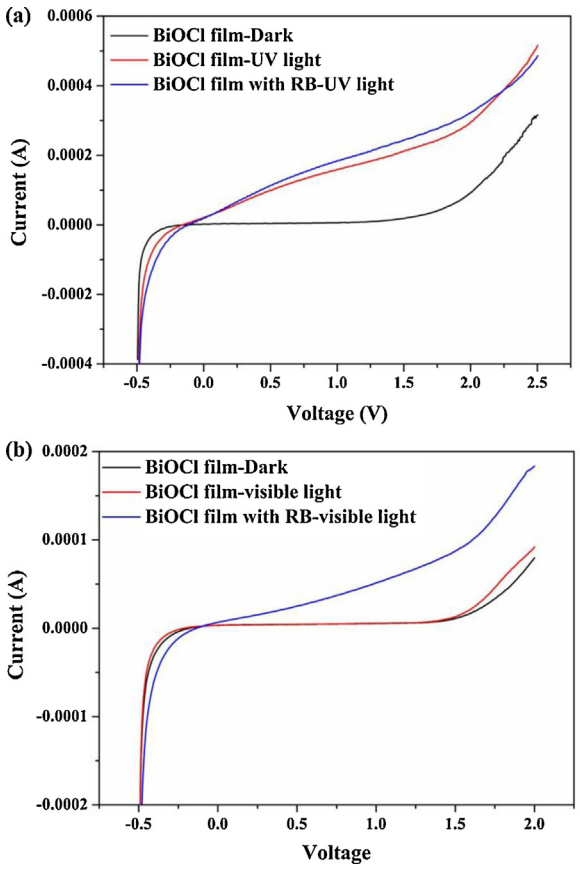

Fig. 10. Photo generated current obtained by the BiOCl film with and without RB adsorption under (a) UV and (b) visible light irradiation.

during the photocatalytic degradation. The UV–vis spectra of RB solution with different irradiation time using BiOCl film under UV and visible light are shown in Fig. S7. Except the peaks of chromophoric group (—C=N— at 563 nm), the UV–vis absorption peaks of aromatic ring (259 nm and 284 nm) also decreased with the degradation of RB, especially under UV light. As well known, total organic carbon (TOC) value is widely used to determine the mineralization standard of organic compound and examine the water quality. The TOC removal efficiencies of RB solution obtained by the BiOCl film under UV and visible light are also shown in Fig. 8 (the red line). The TOC removal efficiency increased with degradation time increasing, however compared with that of color, it was lower especially under visible light, only 70% TOC was removed in 180 min. The result indicates that the photocatalytic activity of BiOCl film is better under UV light than that under visible light, degradation intermediates such as small molecule aromatic hydrocarbons and organic acids still exists and total mineralization of RB requires a longer time [32,33].

3.5. Photocatalytic mechanisms of BiOCl film

The photo-generated electrons during the reaction under UV and visible light were detected by the linear sweep voltammograms with and without RB adsorption on the surface of BiOCl film. The results are shown in Fig. 10, when there was no RB adsorbed on the surface of BiOCl film, the photo-generated current was observed under UV light irradiation and it increased with the increasing of applied voltage (Fig. 10a). However there was not any photo-generated current under visible light irradiation at the voltage range from 0 V to 1.5 V (Fig. 10b). This result coincides with the UV–vis DRS (Fig. 7), which indicates that the BiOCl film that prepared can only be excited by UV light and generates electron–hole pairs, while it can hardly be excited by visible light due to the wide band gap energy. However when there was RB adsorbed on the surface of BiOCl film, compared with dark current, significant photo-generated current was observed under visible light irradiation (Fig. 10b). Because the BiOCl film can hardly be excited by visible light to generate electron–hole pairs, the photo-generated electrons may mainly come from the excitation of RB and dye photosensitization on the surface of the film.

In order to determine the active species generated during the RB photocatalytic degradation on BiOCl film under UV and visible light, different trapping agents were dissolved in the reaction solution before light irradiation. As shown in Fig. 11a, the RB color removal efficiency was significantly suppressed after trapping $O_2^{\bullet -}$ by adding BQ. Trapping photo-generated holes and $^{\bullet}OH$ with KI and TBA, respectively, also exhibited restraining effect on RB color removal under UV light, however there were weaker or no influence under visible light. It can be discovered that the holes, $^{\bullet}OH$ and $O_2^{\bullet -}$ are all generated during the reaction under UV light, however only $O_2^{\bullet -}$ radical is the main active specie during the visible light photocatalytic degradation process.

According to the results of photo-generated current and active species trapping experiments, the plausible reaction mechanisms under UV and visible light on the surface of BiOCl film can be proposed in Fig. 11b and Fig. 11c, respectively. When UV light irradiated on the surface of BiOCl film, BiOCl was excited to generate electron–hole pairs (Fig. 11b). The electrons in the conduction band of BiOCl reacted with O_2 to generate $O_2^{\bullet -}$ and further oxidized RB on the surface of the film. Meanwhile the photo-generated holes in the valence band oxidized RB that adsorbed directly or to oxidized H_2O molecules to generate $^{\bullet}OH$ radicals with strong oxidative power and further oxidized RB indirectly. Many researchers have reported that the presence of internal electric fields between $[Bi_2O_2]$ and $[Cl_2]$ in the layered structure BiOCl (Fig. S3) are favorable for the efficient photoinduced electron–hole separation and transfer to the surface to degrade the adsorbed dye molecule [10,34], which causes the better UV photocatalytic performance than TiO_2 film on RB degradation.

When visible light irradiated, dye sensitization took place to degrade RB that adsorbed on the surface of BiOCl film. As shown in Fig. 11c, the RB adsorbed on the surface of BiOCl was excited by visible light irradiation to generate electrons and then the electrons were injected from the excited RB to the conduction band of BiOCl where the electrons were further scavenged by molecular oxygen to yield the $O_2^{\bullet -}$ radical anions and oxidized RB molecules. The existence of BiOCl catalyst was a prerequisite and played the important role of electron carrier and acceptor. Because the increase in both the dye adsorption amount and strength can promote the electron transfer from the excited dyes to catalyst [35,36], the strong adsorption performance of layered structure BiOCl film promotes both the adsorption amount and adsorption strength for RB dye, which allows more efficient transport for the injected electrons from the excited RB to BiOCl film, leading to a great visible light photocatalytic performance. The photographic image of BiOCl film with RB adsorbed is shown in Fig. S4(c), the color of the film turned from white to rose red. The morphological views of the BiOCl hierarchical structure with RB adsorbed are shown in Fig. 12 and compared with Fig. 3, the surface of the BiOCl film was much more unclear due to the large amount of RB adsorption.

3.6. Stability of the BiOCl film

Attempts were made in this study to determine the stability of the BiOCl film, which is an important factor to take into consideration in real industrial application. Five runs of photocatalytic

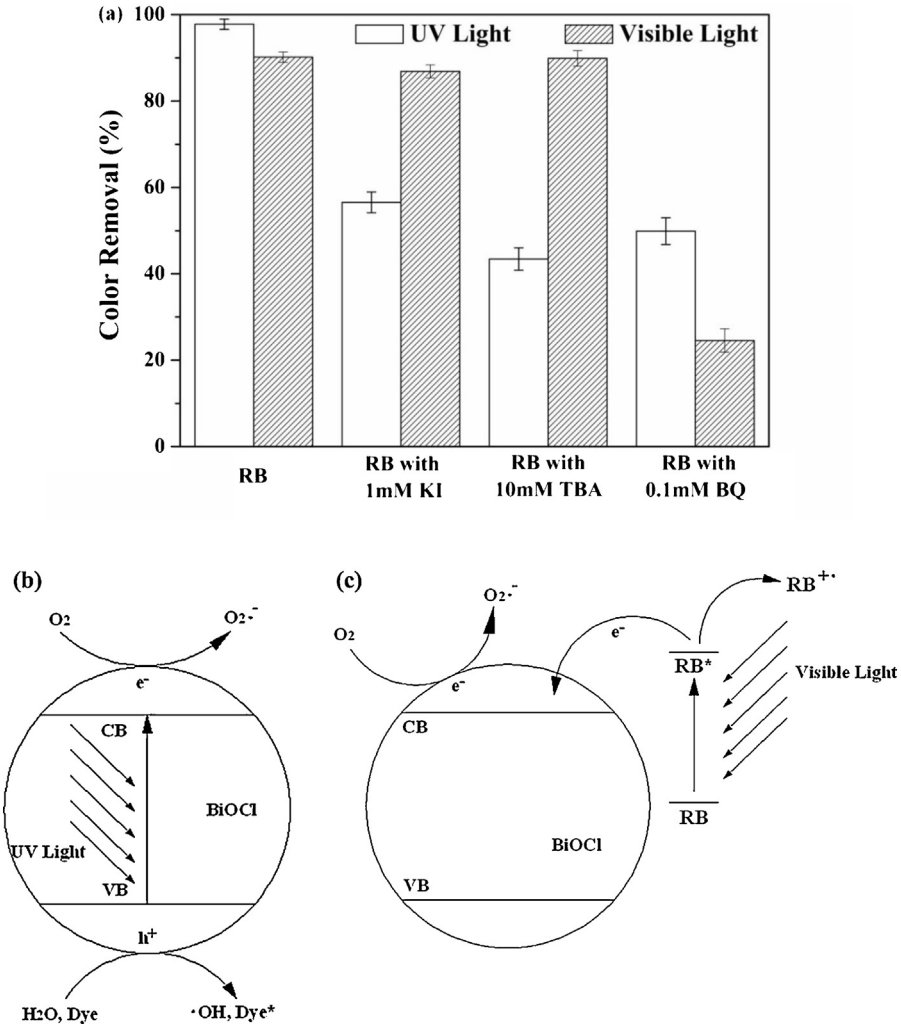

Fig. 11. Photocatalytic mechanism for BiOCl film: (a) trapping experiment of active species during the UV and visible light photocatalytic process (KI, h^+ trapping agent; TBA, $^{\bullet}OH$ trapping agent; BQ, $O_2^{\bullet-}$ trapping agent). (b)(c) Photocatalytic mechanism schemes of BiOCl film under UV and visible light irradiation.

process were repeated on one BiOCl film to treat 50 mL 5 mg L^{-1} RB solution under UV and visible light irradiation respectively. Each UV degradation process was operated for 2 h and the sample was collected at a time interval of 15 min. While each visible light degradation experiment was operated for 3 h and the sample was collected at a time interval of 20 min. As shown in Fig. 13, similar RB color removal efficiency at the same time interval during the repeated process demonstrates excellent stability and reliability of the BiOCl film.

3.7. Photocatalytic activity of other dye solutions

50 mL 5 mg L^{-1} other dye solutions, including Methylene Blue (MB), Basic Orange (BO), Methyl Orange (MO) and Reactive Brilliant Red X-3B (RBR) were also used to be degraded by BiOCl film under UV and visible light and the results are shown in Fig. 14. The BiOCl film exhibited excellent photocatalytic activity when UV light irradiated, 100% color removal efficiency were achieved in 120 min for all four kinds of dyes. When visible light irradiated, the color

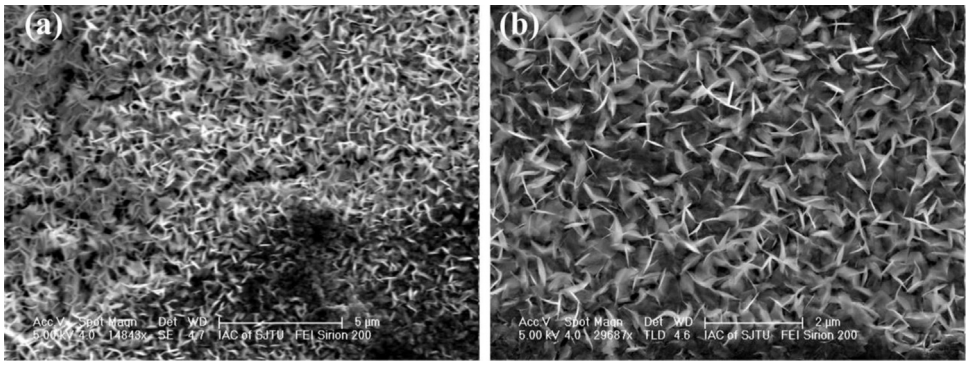

Fig. 12. FESEM images of BiOCl film with RB adsorbed on the surface, (a) with low magnification and (b) with high magnification.

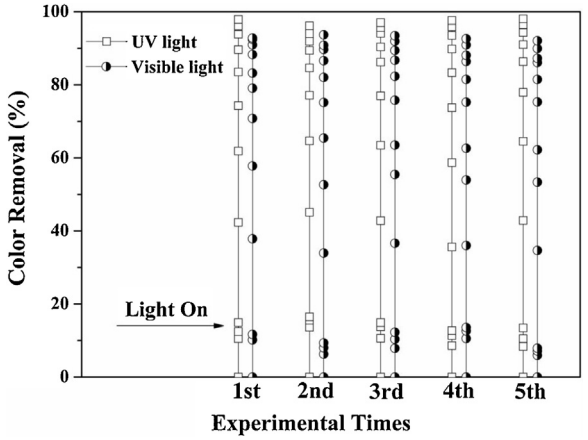

Fig. 13. Repeated decolorization of 50 mL 5 mg L^{-1} RB solution with BiOCl film under UV light and visible light.

removal efficiencies of different dyes were different. More than 85% BO and 75% MB were removed in 180 min under visible light, while only 50% MO and less than 30% RBR were removed in the same time period. It is known that a dye photosensitization mechanism is closely related to the dye structural stability, the dye absorbance and the adsorption capacity of photocatalyst [35,36]. Cationic dyes (RB, BO and MB) are much easier to adsorb on the surface of the prepared BiOCl film than the anionic dyes (MO and RBR), which causes the differences of color removal efficiency under visible light irradiation. Meanwhile Ji et al. also found that the photocatalytic degradation rate is related to the frontier orbital energy of the dyes, that is, highest occupied molecular orbital (HOMO) and lowest unoccupied molecular orbital (LUMO). The higher is the LUMO, the more favorable for the electrons to transfer from dye molecules to the conduction band of semiconductors and thus facilitating the photodegradation reaction process [37]. The influence of different dyes on the photodegradation efficiency with BiOCl film that prepared under UV and visible light will be deeply investigated in our future work.

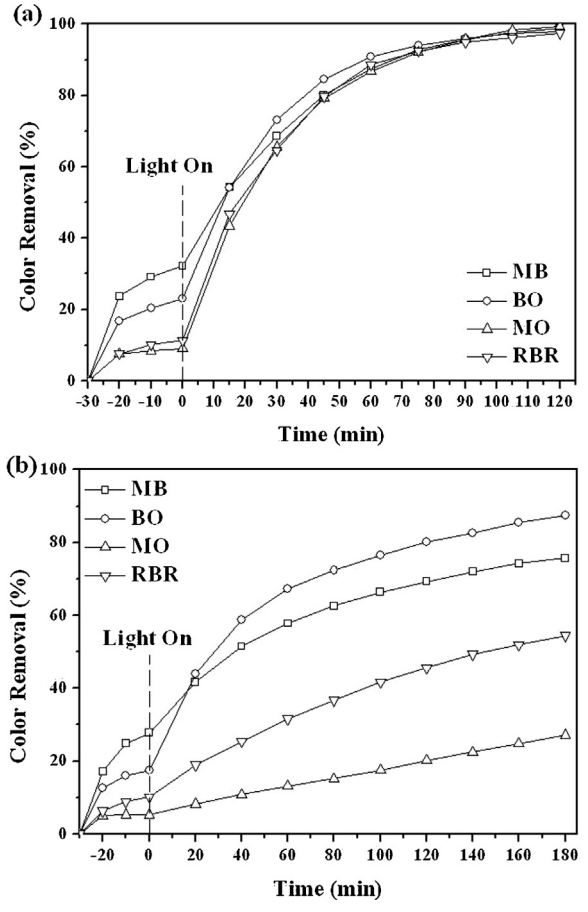

Fig. 14. Photodegradation of 50 mL 5 mg L^{-1} MB, BO, MO and RBR dye solution with BiOCl film under (a) UV and (b) visible light irradiation.

4. Conclusion

A BiOCl film with hierarchical nanostructure on a Ti substrate was prepared by a facile method, using Bi_2O_3 film reacted with Cl^- in acidic condition. The as-prepared BiOCl film was characterized by X-ray diffraction (XRD), field emission scanning electron microscope (FESEM), high-resolution transmission electron microscopy (HRTEM) and UV–vis diffuse reflectance spectra (UV–vis DRS). The growth mechanism of the flowerlike hierarchical structure BiOCl film was a nucleation–dissolution–recrystallization process according to the FESEM at different reaction time. 50 mL 5 mg L^{-1} Rhodamine B (RB) solution was used to be degraded using the BiOCl film under UV and visible light irradiation to evaluate its photocatalytic activity. More than 10% RB could adsorb on the surface of the film before the light on. Nearly 100% and more than 90% RB could be removed under UV and visible light in 120 min and 180 min, which were much better than that obtained by TiO_2 film, especially under visible light. Except color, TOC could also be removed efficiently. More than 90% and 70% TOC removal efficiency could be achieved under UV and visible light in the same condition. The RB photocatalytic degradation mechanisms were analyzed by degrading colorless salicylic acid (SA) instead of RB, detecting photo-generated current and adding active species trapping agents. The results suggested that the prepared BiOCl film exhibited high activity for direct semiconductor photoexcitation RB degradation under UV light, while it also possessed superior activity for indirect RB photosensitization degradation under visible light. Other dye solutions, including Methylene Blue (MB), Basic Orange (BO), Methyl Orange (MO) and Reactive Brilliant Red X-3B (RBR), were also used to be treated under UV and visible light in the same condition, the BiOCl film exhibited excellent photocatalytic activity for all these dyes and possessed the potential application in wastewater treatment.

Acknowledgments

This work was supported by the Natural Science Foundation of China (Project Nos. 20937003 and 50878126) and Ph.D. Program Foundation of Ministry of Education of China (Project No. 20090073110033).

Appendix A. Supplementary data

Supplementary data associated with this article can be found, in the online version, at http://dx.doi.org/10.1016/j.apcatb.2013.04.005.

References

[1] A. Hameed, T. Montini, V. Gombac, P. Fornasiero, Journal of the American Chemical Society 130 (2008) 9658–9659.
[2] X. Chang, J. Huang, C. Cheng, Q. Sui, W. Sha, G. Ji, S. Deng, G. Yu, Catalysis Communications 11 (2012) 460–464.
[3] Z. Zhang, W. Wang, M. Shang, W. Yin, Journal of Hazardous Materials 177 (2010) 1013–1018.
[4] B. Zhou, X. Zhao, H. Liu, J. Qu, C.P. Huang, Applied Catalysis B: Environmental 99 (2012) 214–221.

[5] J. Geng, W.H. Hou, Y.N. Lv, J.J. Zhu, H.Y. Chen, Inorganic Chemistry 44 (2005) 8503–8509.
[6] A.M. Kusainova, P. Lightfoot, W. Zhou, S.Y. Stefanovich, A.V. Mosunov, V.A. Dolgikh, Chemistry of Materials 13 (2001) 4731–4737.
[7] X. Lin, Z. Shan, K. Li, W. Wang, J. Yang, F. Huang, Solid State Sciences 9 (2007) 944–949.
[8] Z. Deng, F. Tang, A.J. Muscat, Nanotechnology 19 (2008) 295705.
[9] M.A. Gondal, X.F. Chang, Z.H. Yamani, Chemical Engineering Journal 165 (2010) 250–257.
[10] K.L. Zhang, C.M. Liu, F.Q. Huang, C. Zheng, W.D. Wang, Applied Catalysis B: Environmental 68 (2006) 125–129.
[11] J. Jiang, K. Zhao, X. Xiao, L. Zhang, Journal of the American Chemical Society 134 (2012) 4473–4476.
[12] B. Pare, B. Sarwan, S.B. Jonnalagadda, Journal of Molecular Structure 1007 (2012) 196–202.
[13] K. Zhang, J. Liang, S. Wang, J. Liu, K. Ren, X. Zheng, H. Luo, Y. Peng, X. Zou, X. Bo, J. Li, X. Yu, Crystal Growth & Design 12 (2012) 793–803.
[14] J. Xiong, G. Cheng, G. Li, F. Qin, R. Chen, RSC Advances 1 (2011) 1542–1553.
[15] Y. Lei, G. Wang, S. Song, W. Fan, H. Zhang, CrystEngComm 11 (2009) 1857–1862.
[16] C. Wang, C. Shao, Y. Liu, L. Zhang, Scripta Materialia 59 (2008) 332–335.
[17] J. Ma, X. Liu, J. Lian, X. Duan, W. Zheng, Crystal Growth & Design 10 (2010) 2522–2527.
[18] H. Peng, C.K. Chan, S. Meister, X.F. Zhang, Y. Cui, Chemistry of Materials 21 (2009) 247–252.
[19] S. Cao, C. Guo, Y. Lv, Y. Guo, Q. Liu, Nanotechnology 20 (2009) 275702.
[20] S. Wu, C. Wang, Y. Cui, W. Hao, T. Wang, P. Brault, Materials Letters 65 (2011) 1344–1347.
[21] X. Zhang, X. Liu, C. Fan, Y. Wang, Y. Wang, Z. Liang, Applied Catalysis B: Environmental 132–133 (2013) 332–341.
[22] K. Li, C. Yang, Y. Xu, D. Ying, Y. Wang, J. Jia, Chemical Engineering Journal 211-212 (2012) 208–215.
[23] Y. Xu, Y. He, X. Cao, D. Zhong, J. Jia, Environmental Science & Technology 42 (2008) 2612–2617.
[24] K. Li, Y. He, Y. Xu, Y. Wang, J. Jia, Environmental Science & Technology 45 (2011) 7401–7407.
[25] K. Li, C. Yang, Y. Wang, J. Jia, Y. Xu, Y. He, AIChE Journal 58 (2012) 2448–2455.
[26] M. Yin, Z. Li, J. Kou, Z. Zou, Environmental Science & Technology 43 (2009) 8361–8366.
[27] C. Pan, Y. Zhu, Environmental Science & Technology 44 (2010) 5570–5574.
[28] L. Ye, J. Liu, C. Gong, L. Tian, T. Peng, L. Zan, ACS Catalysis 2 (2012) 1677–1683.
[29] H. Li, Z. Bian, J. Zhu, D. Zhang, G. Li, Y. Huo, H. Li, Y. Lu, Journal of the American Chemical Society 129 (2007) 8406–8407.
[30] Y. Huo, J. Zhang, M. Miao, Y. Jin, Applied Catalysis B: Environmental 111–112 (2012) 334–341.
[31] G. Dukovic, F. Wang, D. Song, M.Y. Sfeir, T.F. Heinz, L.E. Brus, Nano Letters 5 (2005) 2314–2318.
[32] P. Lei, C. Chen, J. Yang, W. Ma, J. Zhao, L. Zhang, Environmental Science & Technology 39 (2005) 8466–8474.
[33] Z. Zainal, C.Y. Lee, M.Z. Hussein, A. Kassim, N.A. Yusof, Journal of Hazardous Materials 146 (2007) 73–80.
[34] H. An, Y. Du, T. Wang, C. Wang, W. Hao, J. Zhang, Rare Metals 27 (2008) 243–250.
[35] T. Wu, G. Liu, J. Zhao, H. Hidaka, N. Serpone, The Journal of Physical Chemistry B 102 (1998) 5845–5851.
[36] J. Zhao, T. Wu, K. Wu, K. Oikawa, H. Hidaka, N. Serpone, Environmental Science & Technology 32 (1998) 2394–2400.
[37] X. Chang, M.A. Gondal, A.A. Al-Saadi, M.A. Ali, H. Shen, Q. Zhou, J. Zhang, M. Du, Y. Liu, G. Ji, Journal of Colloid and Interface Science 377 (2012) 291–298.